Strong Impact of the Oxygen Content in $Na_3V_2(PO_4)_2F_{3-y}O_y$ ($0 \leq y \leq 0.5$) on its Structural and Electrochemical Properties

Thibault Broux [a,b,e], Tahya Bamine [a,e], François Fauth [c], Laura Simonelli [c], Wojciech Olszewski [c,d], Carlo Marini [c], Michel Ménétrier [a,e], Dany Carlier [a,e], Christian Masquelier [b,e,f] and Laurence Croguennec [a,e,f,1]

[a] *CNRS, Univ. Bordeaux, Bordeaux INP, ICMCB UPR 9048, F-33600 Pessac, France.*

[b] *Laboratoire de Réactivité et de Chimie des Solides, CNRS-UMR#7314, Université de Picardie Jules Verne, F-80039 Amiens Cedex 1, France*

[c] *CELLS - ALBA synchrotron, E-08290 Cerdanyola del Vallès, Barcelona, Spain*

[d] *Faculty of Physics, University of Bialystok, 1L K. Cio lkowskiego Str., 15-245 Bia lystok, Poland*

[e] *RS2E, Réseau Français sur le Stockage Electrochimique de l'Energie, FR CNRS 3459, F-80039 Amiens Cedex 1, France*

[f] *ALISTORE-ERI European Research Institute, FR CNRS 3104, F-80039 Amiens Cedex 1, France*

Abstract

Polyanionic materials such as $Na_3V_2(PO_4)_2F_{3-y}O_y$ ($0 \leq y \leq 2$) are of high interest as positive electrode for Na-ion batteries since they offer competitive electrochemical performances compared to sodiated transition metal oxides. The composition $Na_3V_2(PO_4)_2F_3$ ($y = 0$) has the highest theoretical energy density among the series but surprisingly a lot of discrepancies are reported throughout the literature considering its structure and its electrochemical properties. We will show that most of the compounds reported as being $Na_3V^{III}_2(PO_4)_2F_3$ are in fact slightly oxidized due to synthesis conditions resulting in a partial oxygen substitution for fluorine. In order to get an in-depth understanding of this system, a series of compositions $Na_3V_2(PO_4)_2F_{3-y}O_y$ ($0 \leq y \leq 0.5$, *i.e.* near the fluorine-rich composition) was synthesized and characterized combining synchrotron X-ray diffraction, X-ray absorption spectroscopy, solid state nuclear magnetic resonance spectroscopy and galvanostatic electrochemical tests. The structural features and electrochemical signatures of these oxidized compounds will be carefully compared to those recently obtained for $Na_3V^{III}_2(PO_4)_2F_3$ by Bianchini *et al.*

[1] Corresponding author (L. Croguennec): Laurence.Croguennec@icmcb.cnrs.fr

Introduction

Up to now, Li-ion batteries have been shown to be the most efficient technology for the electrochemical energy storage developed for portable and automotive applications.[1] In order to overcome drawbacks associated to the availability and prize of lithium resources,[2] and thus to develop alternatives to Li-ion batteries for targeted applications, the Na-ion technology appears to be a short term reasonable option given that it is similar in terms of materials used and industrial processing.[3] Despite several advantages including lower price and very large earth-abundance of sodium important drawbacks must be overcome to ensure a possible future for the Na-ion technology: a less negative standard reduction potential (-2.7 V *vs* SHE for the Na^+_{aq}/Na against -3.04 V for the Li^+_{aq}/Li one) and a higher molecular mass both contributing to reduce the energy density compared to Li-ion material with the same composition.

Among several polyanionic-based electrode materials,[4-10] one of the most promising family turns out to be the sodium-vanadium fluorophosphate compounds $Na_3V_2(PO_4)_2F_{3-y}O_y$ (also called $NVPF_{3-y}O_y$ in this paper) where y can vary from 0 to 2[11-19] also reported as $Na_3V_2O_{2y}(PO_4)_2F_{3-2y}$[11-12] and $Na_3(VO_{1-y}PO_4)_2F_{1+2y}$[14] where y can vary from 0 to 1. For instance in $Na_3V_2(PO_4)_2F_3$ ($y = 0$, $NVPF_3$) the extraction of 2 Na^+ ions has been experimentally demonstrated with two main voltage-composition plateaus at around 3.7 and 4.2 V *vs* Na^+/Na and a theoretical energy density of 507 Wh/kg[18, 20-21] (128 Ah/kg at an average potential of 3.95 V) competitive with that delivered by $LiFePO_4$ in Li-ion batteries. Several studies have been performed recently which revealed significant discrepancies in the structural description and electrochemical properties of $NVPF_3$. For instance, unit cell volumes ranging from 871 to 878 $Å^3$ were reported[18, 20] whereas the phase diagram observed upon cycling was described either as complex with a series of two-phase reactions and solid solution[15] or only as a solid solution.[22] It clearly stands out that some subtle differences in as-prepared compositions have to be clarified considering especially the effect on the structural and electrochemical features of a possible partial substitution of oxygen for fluorine and thus of a mixed valence state for vanadium ($V^{3+,4+}$) induced by synthesis conditions.

More precisely, the structure of $NVPF_{3-y}O_y$ ($0 \leq y \leq 2$) consists of a tridimensional framework of $V_2O_8F_{3-y}O_y$ bi-octahedra which are connected by PO_4 tetrahedra. When $y > 0$ the substitution of oxygen for fluorine occurs at the apex of the $V_2O_8F_{3-y}O_y$ bi-octahedra, inducing the formation of shorter covalent vanadyl-type bonds as terminal bonds and thus the contraction of the bi-octahedra. Regardless the F/O ratio, the framework of $NVPF_{3-y}O_y$ ($0 \leq y \leq 2$) is characterized by large tunnels where Na^+ ions are mobile upon the intercalation and deintercalation reactions. To date, two space groups have been used to describe the crystal structure at 298 K of the whole series $NVPF_{3-y}O_y$ ($0 \leq y \leq 2$): $P4_2/mnm$ and $Amam$. Recently it has been evidenced by Bianchini *et al.*[16] that the well-known structure of $NVPF_3$ described by Le Meins et *al.* in the tetragonal space group $P4_2/mnm$[23] turned out to be not appropriate since a subtle orthorhombic distortion had to be considered. As shown in **Figure 1** this distortion is linked to

the sodium distribution only, and does not affect significantly the framework. Three sodium sites (one in 4c and two in 8f Wyckoff positions) are observed in the *Amam* space group, and only two sites (in 8i Wyckoff positions) in the $P4_2/mnm$ space group. Since all $NVPF_{3-y}O_y$ compositions (*i.e.* with a different F/O ratio) are reported to be tetragonal[12, 14, 24] it is crucial to determine if this distortion subsists in oxidized compounds, its impact on the sodium distribution, but also more extensively the relationship between composition, structure and electrochemical properties. Furthermore, the creation of a more covalent bond within the transition metal environment induces a decrease in the average operating voltage which is important regarding electrochemical performance. In other words, a deviation from the "ideal" $y = 0$ composition is expected to be associated to a loss of performance hence the importance of studying this feature for $Na_3V_2(PO_4)_2F_3$.

Here a series of six partially oxidized $Na_3V_2(PO_4)_2F_{3-y}O_y$ compositions with y ranging from 0 ($NVPF_3$) to 0.5 ($NVPF_{2.5}O_{0.5}$) has been prepared through a two-step solid state synthesis method in order to control the F/O ratio that governs the vanadium initial oxidation state: from +3 for $y = 0$ to +3.25 for $y = 0.5$. This study gives new insights into slightly oxidized $NVPF_{3-y}O_y$ compositions and helps conciliating all the discrepancies observed in the literature and arising in fact from a partial oxidation of the as-prepared material.

Experimental

$Na_3V_2(PO_4)_2F_{3-y}O_y$ ($0 \leq y \leq 0.5$) powders were prepared by a two-step solid-state reaction using stoichiometric amounts of $V^{V}OPO_4$, $V^{III}PO_4$, NaF (Sigma-Aldrich; ≥ 99 %), and Na_2CO_3 (Riedel-de Haën; 99.8 %) as precursors. $V^{V}OPO_4$ and $V^{III}PO_4$ were prepared using stoichiometric amounts of V_2O_5 (Sigma-Aldrich; ≥ 99.6 %) and $NH_4H_2PO_4$ (Sigma-Aldrich; ≥ 99.99 %), according to one and two-step solid-state reactions respectively.

High resolution Synchrotron powder X-ray diffraction (SXRD) data were collected using the MSPD diffractometer at ALBA (Barcelona, Spain). The powders were placed in a 0.5 mm diameter capillary and data recorded in Debye-Scherrer geometry with a wavelength of 0.9540 Å in the 2θ angular range of 1 – 70 ° with a 0.005 ° step and an accumulation time of 6 minutes. As already reported by Bianchini *et al.*[16] for the structural determination of $Na_3V^{III}_2(PO_4)_2F_3$ ($y = 0$), the use of very high angular resolution techniques is essential as a very small orthorhombic distortion exists. Their detection is important to reveal significant changes in the distribution of sodium ions within the 3D framework and thus in the interpretation of electrochemical processes.

The chemical composition of $NVPF_{3-y}O_y$ in Na, V and P was confirmed by inductively coupled plasma-optical emission spectroscopy (ICP-OES) using a Varian Model 720-ES spectrometer after complete dissolution of the powder into a hydrochloric acid (HCl) solution.

Vanadium K-edge X-ray absorption spectra were collected at room temperature in transmission mode using three ionization chambers mounted in series for simultaneous measurements of the sample and reference at the beamline CLÆSS at ALBA (Barcelona, Spain). The synchrotron radiation emitted by the CLÆSS multipole wiggler was first vertically collimated and then monochromatised by a Si(111) double-crystal monochromator. The monochromatised beam was then focused down to 100 x 200 μm^2 at the sample position by a toroidal focusing mirror. Higher harmonic contributions to the selected energy were suppressed by setting the coating and the rejecting angle of the two mirrors. Powder samples were mixed uniformly in boron nitride matrix and pressed into pellets of 13 mm diameter, for obtaining the vanadium K-edge step close to 1. Several X-ray absorption scans were collected to ensure the reproducibility of the spectra and to obtain high signal to noise ratio.

^{23}Na MAS NMR spectra were recorded on a Bruker Avance 500 MHz spectrometer (132.3 MHz resonance frequency for ^{23}Na) using a standard Bruker 2.5 mm MAS probe with a 30 kHz typical spinning frequency. A short pulse length of 1 µs corresponding to a selective $\pi/12$ pulse determined using an aqueous 0.1 mol/L NaCl solution was employed. The spectral width was set to 1 MHz and the recycle time to $D_0 = 0.5$ s, long enough to avoid T1 saturation effects. The baseline distortions resulting from the spectrometer dead time (5-10 µs) were removed computationally using a polynomial baseline correction routine. The 0 ppm external reference was a 0.1M NaCl aqueous solution. ^{31}P MAS NMR spectra were recorded on a Bruker Avance III 100 MHz spectrometer (40.6 MHz resonance frequency for ^{31}P), using a standard Bruker 2.5 mm MAS probe with a 30 kHz typical spinning frequency. A Hahn echo sequence was used with a 90 ° pulse of 1.1 µs. A recycle delay of 1 s was typically used. The 0 ppm external reference was H_3PO_4 85 % sigma Aldrich.

Scanning electron microscopy (SEM) analysis of metallized samples (Pd-deposited) was performed using a Hitachi Model S-4500 microscope.

Electrochemical tests were performed in CR2032-type coin cells. The positive electrodes were prepared from a slurry made of 80 wt% $Na_3V_2(PO_4)_2F_{3-y}O_y$ ($0 \leq y \leq 0.5$), 10 wt% carbon black, and 10 wt% polyvinylidene fluoride (PVDF) dispersed in N-methyl-2-pyrrolidone (NMP), casted on an Al foil and dried at 80 °C overnight. The loading of the active material on the electrodes was around 2.5 mg/cm². The negative electrode was sodium metal, whereas the electrolyte was home-made from a 1 M solution of $NaPF_6$ (Strem Chemical; 99%) in ethylene carbonate and dimethyl carbonate (EC:DMC = 1:1) with 3 wt% of fluoroethylene carbonate (FEC) as additive. The electrochemical cells were charged and discharged in galvanostatic mode, at a C/20 between 2.5 and 4.3 V *vs* Na^+/Na corresponding to the exchange of 0.1 mol of sodium ions/electrons per hour.

Results and discussion

1. Syntheses of the series of $Na_3V_2(PO_4)_2F_{3-y}O_y$ ($0 \leq y \leq 0.5$) compositions

The synthesis of $Na_3V_2(PO_4)_2F_{3-y}O_y$ ($0 \leq y \leq 0.5$) was performed in two steps using conditions similar to those reported by Park *et al.*[14] with $V^{V}OPO_4$ and $V^{III}PO_4$ used as intermediate precursors. The V^{III} phosphate precursor was prepared by mixing stoichiometric amounts of $V^{V}_2O_5$ and $NH_4H_2PO_4$ in a high energy ball mill for 90 min. This mixture was then continuously heated under pure H_2 to ensure a complete reduction of V^{V} to V^{III} at 300 °C for 5 h (with a heating ramp of 0.5 °C/min) and at 800 °C for 5 h (with a heating ramp of 2 °C/min), before being cooled down to room temperature at 3 °C/min. VPO_4 is obtained without any carbon coating, contrary to that prepared by Park *et al.* using carbothermal reduction conditions. $V^{V}OPO_4$ was obtained by the oxidation of $V^{III}PO_4$ in air by a thermal treatment at 700 °C for 5 h (heating/cooling rate of 3 °C/min). $Na_3V_2(PO_4)_2F_{3-y}O_y$ compounds were finally obtained according to the following reaction, mixing stoichiometric amounts of V^{III} and V^{V} precursors in order to control the average oxidation state of vanadium with NaF and Na_2CO_3 in in order to control the F/O ratio in a high energy ball mill for 90 min, and then sintering this mixture under argon at 750 °C for 2 h (heating/cooling rate of 3 °C/min):

$$(3-y)NaF + y/2Na_2CO_3 + (2-y)V^{III}PO_4 + yV^{V}OPO_4 \rightarrow Na_3V^{III}_{2-y}(V^{IV}O)_y(PO_4)_2F_{3-y} + y/2CO_2 + y/4O_2$$

As previously reported by Bianchini *et al.*[16] the powders were washed for around 24 h under stirring in water in order to eliminate minor impurities soluble in water such as Na_3VF_6 and $Na_5P_3O_{10}$. The resulting powders were then dried under vacuum for 24 h at 80 °C. The color of the resulting powders gradually varies from dark green for the $y = 0$ compound to light green for $y = 0.5$ which is consistent with previous observations.[26]

The SXRD patterns of the six samples thus obtained are compared in **Figure 2**. All the main diffraction lines can be indexed in unit cells described in the *Amam* space group similar to that determined by Bianchini *et al.* for $Na_3V_2(PO_4)_2F_3$.[16] No superstructure peaks are observed suggesting neither anionic nor electronic order. Close inspection of the SXRD data especially for the angular ranges [9.9 - 10.4°] and [24.15 - 24.55°] highlights a continuous decrease of the *c* cell parameter with increasing *y*, as the (002) line shifts to higher 2θ angles. In addition, the (400) and (040) reflections tend to merge as a unique peak from $y = 0.4$ suggesting a decrease/disappearance of the orthorhombic distortion with increasing *y*. The cell parameters determined for the six $NVPF_{3-y}O_y$ samples from the profile matching refinement of their SXRD data are reported in **Figure 3** and in **Table 1**. As expected, the $y = 0$ end member has similar cell parameters to those already reported by Bianchini *et al.*[16] for $Na_3V_2(PO_4)_2F_3$ (a = 9.02847(3) Å, b = 9.04444(3) Å and c = 10.74666(6) Å) and once again the orthorhombic distortion with a b/a ratio of 1.002 is confirmed. The *c* cell parameter and unit cell volume V of $Na_3V_2(PO_4)_2F_{3-y}O_y$ are decreasing from 10.7538 to 10.6863 Å and from 878.393 to 872.604 $Å^3$ respectively, in good

agreement with a partial oxidation of V^{III} to V^{IV} due to an increasing substitution of oxygen (O^{2-}) for fluorine (F^-). As expecting from the continuous merging of the (040) and (400) lines with increasing *y*, the *b*/*a* ratio decreases from 1.002 for $y = 0$ to 1.0002 for $y = 0.5$ questioning the validity of the orthorhombic distortion for the most oxidized composition ($y = 0.5$). It is interesting to compare these unit cell parameters to the large panel of units cells reported in the literature for compositions announced to be $Na_3V_2(PO_4)_2F_3$, whereas they are most probably (slightly) oxidized.[6, 8, 16-20, 23]

The SXRD patterns exhibit narrower diffraction peaks with increasing *y* ($0.03387(5)° \geq FWHM_{(002)} \geq 0.02853(4)°$ for *y* increasing from 0 to 0.5) and reveal thus a higher crystallinity of the powder obtained in the presence of a larger amount of sodium carbonate Na_2CO_3 used as sodium precursor which might act as a flux for crystalline growth. Indeed, considering the SEM micrographs given as supplementary information (see **figure S1**) a growth of the primary particles is observed as *y* is increasing from 1 to 5 µm approximatively. Careful inspection of these SXRD data reveals also the presence of negligible amounts of remaining impurities in some samples. The small intensity peak observed at $2\theta = 20°$ is attributed to Na_3VF_6 and those observed at $2\theta = 15°$ and 22 ° to $Na_5P_3O_{10}$ (highlighted by ¤ and * respectively in **Figure 2**). Molar ratios of Na/V/P determined by chemical analyses carried out with ICP-OES are in good agreement with the expected chemical formula $Na_3V_2(PO_4)_2F_{3-y}O_y$ (*i.e.* with 1.5Na:1V:1P as reported in **Table 1**). The obtained results of ICP are not affected by the small amount of impurity considering uncertainty intrinsic to the measurement.

In the following, in-depth structural characterization using synchrotron X-ray diffraction is detailed for the series of compounds $Na_3V_2(PO_4)_2F_{3-y}O_y$ ($0 \leq y \leq 0.5$).

2. Structural study

The structural descriptions used in the following for Rietveld refinements derive from those reported by Le Meins *et al.*[23] and Bianchini *et al.*[16] for the $y = 0$ composition and already described in **Figure 1**. The analysis of the $y = 0.5$ sample is presented in details in the following. As depicted in **Figure 4** the full pattern matching refinements (limited to the determination of the profile and unit cell parameters), considering the unit cell description of $NVPF_{2.5}O_{0.5}$ either in $P4_2/mnm$ or *Amam* space groups lead to similar agreement factors: $\chi^2 = 4.14$ and 4.33 respectively. In order to reach the best structural description, systematic Rietveld refinements combined with Fourier difference map calculations were carried out to assert how the F/O ratio affects the structure.

In a first step, only the framework $V_2(PO_4)_3F_{3-y}O_y$ was considered in order to localize from scratch the Na^+ ions by the analysis of the Fourier difference maps. As expected, major residues were observed that correspond to Na^+ ions as presented in **Figure 5**. A rather good minimization of the residues is achieved considering the two structural descriptions already reported for $NVPF_3$ in *Amam*[16] and $P4_2/mnm$[23] space

groups. However, significant residues are still observed between crystallographic Na sites indicating a lack of accuracy in our structural model. A further decrease of the residue accompanied with an increase of the refinement quality is achieved adding one additional site in both cases (see **Figure 5**). Even if there are still some small residues in the Fourier difference maps, adding additional sites did not lead to a significant improvement of the refinement quality. Note that the resulting Na^+ ions distributions displayed in **Figure 5** are close to each other as sodium ions are located within the whole torus provided by the polyanionic framework similarly to what has been reported before for the high temperature structure of $NVPF_3$.[16]

Considering the quality of the refinement and the chemical bonds associated to the framework, the orthorhombic unit cell appears to be the most relevant to describe the structure of the $y = 0.5$ oxidized compound. First, the agreement factors are better for a similar number of refined parameters: $\chi^2 = 9.07$ and $R_{Bragg} = 5.94$ in the *Amam* space group compared to 10.8 and 6.68 respectively in the $P4_2/mnm$ space group. Besides, careful analysis of the structural parameters obtained for the two structural descriptions (gathered in **Tables S1, S2** and **S3**) reveals that for the structure described in the tetragonal symmetry the P-O interatomic distances are significantly out the range expected for highly covalent bonds in phosphate groups (*i.e.* [1.5 - 1.6 Å]): this result supports strongly the description in the orthorhombic symmetry. Indeed, in the $P4_2/mnm$ unit cell two PO_4 groups are present, the first one being fully isotropic with a single P(1)-O(1) interatomic distance of 1.521(5) Å and the second one being highly distorted with two short P(2)-O(2) interatomic distances of 1.459(5) Å and two long P(2)-O(3) interatomic distances of 1.642(6) Å. For comparison, in the *Amam* unit cell a single PO_4 group is observed with two interatomic distances P(1)-O(1) of 1.534(4) Å and P(1)-O(2) of 1.528(4) Å, consistent with the formation of a highly covalent anionic group. The vanadium environment is very similar in the two structural descriptions, with the equatorial interatomic distances V-O in the typical range of [1.97 - 2.02 Å] and the apical ones around 1.82 Å for the shortest and 2.03 Å for the longest. These features led us to conclude that the *Amam* space group describes also better the structure of $NVPF_{2.5}O_{0.5}$.

As illustrated in **Figure 5**, the Na^+ ions are distributed among four sites in $NVPF_{2.5}O_{0.5}$. Na(1) is localized at the center of a pyramid with an occupancy around 85 %, whereas the three others are in pyramidal (Na(2) and Na(4)) or in capped prismatic (Na(3)) sites but not at their center. Because of their vicinity, to minimize the electrostatic repulsions, neighboring Na(2), Na(3) and Na(4) positions cannot be occupied simultaneously. Besides, for the same reason, the more distant a Na site is from its equivalent position, the more occupied it is.

In conclusion, crystal structure Rietveld refinements of the whole series of compositions $Na_3V_2(PO_4)_2F_{3-y}O_y$ ($0 \leq y \leq 0.5$) have been carried out in the *Amam* space group based on the structure proposed by Bianchini *et al.*[16] with one additional sodium site, Na(4). In every studied compositions it

turns out that this additional site increases significantly the quality of the refinement, with its occupancy increasing up to 16 % for $y = 0.5$.

Oxygen substitution for fluorine is associated to a decrease of the *c* cell parameter. As shown in the inset of **Figure 3**, the *c* parameter is composed of two components ($c = 2h + d$), that are the height of the bi-octahedra (*h*) and the distance between the two terminal fluorine (or oxygen) anions (*d*).[14] From $y = 0$ to 0.5, 2*h* varies from 7.883(2) Å to 7.687(3) Å whereas *d* varies from 2.871(2) Å to 2.999(3) Å. Partial oxygen substitution for fluorine is compensated by a partial oxidation of V^{3+} to V^{4+} and thus by the formation of covalent vanadyl-type bonds $(V^{IV}O)^{2+}$ at the apex of the bi-octahedra, shorter than the ionic bonds V^{III}-F: this evolution explains the decrease of the *h* and *c* parameters (evolution of interatomic distances within vanadium environment are given in Figure S2 and S3). The increase of the *d* parameter is explained by the increase of the distances between the Na^+ ions and the apex of the bi-octahedra as displayed in **Figure 1**, in average from 2.42 to 2.50 Å. That increase is coming from the antagonist effect: the more covalent (*i.e.* the shorter) the bond V-$(O,F)_{apex}$ the more ionic (*i.e.* the longer) the bond Na-(O,F) is. Nevertheless, based on this structural characterization only, no conclusion can be made concerning possible impact of oxygen substitution for fluorine on the sodium mobility within this framework. Indeed, no major changes in the sodium sites occupancy and in the isotopic thermal displacement parameters (Biso) are observed.

3. Spectroscopic study

X-ray absorption near edge structure (XANES):

X-ray absorption spectra were recorded at the vanadium K-edge in order to probe changes on the vanadium oxidation state and local structure as function of the partial oxygen substitution for fluorine in the $Na_3V_2(PO_4)_2F_{3-y}O_y$ ($0 \leq y \leq 0.5$) series of compounds. **Figure 6** displays the spectra recorded for $y = 0$, 0.1, 0.3, 0.4 and 0.5 in which the pre-edge and the main peak are localized at 5470 and 5485 eV respectively. The pre-edge features arise from *1s* to *3d* forbidden transitions that become allowed by orbital *3d-p* hybridizations[27] while their energy positions and intensities distributions are linked to the electronic structure and the local structural environment of the probed element. The strong main-peak arises from the $1s \rightarrow 4p$ dipole allowed transition whereas the features at higher energies are strongly influenced by the local geometry around the absorber mainly determined by multiple scattering contributions.[28-30]

While there is a continuous shift towards higher energy for the rising edge which is in good agreement with the oxidation of vanadium, significant changes are also observed in the pre-edge. From the insets given in **Figure 6**, one can observe that at $y = 0$ the pre-peak is composed by three features located at 5466, 5468, and 5469.5 eV characteristic of the V^{3+} state.[24] By increasing *y*, a feature observed at higher

energy (5469.5 eV) arises which is characteristic of a V^{4+} state.[24] Moreover, a constant growth of the global intensity of the pre-edge is observed as a function of *y*, in good agreement with an increase of the vanadium oxidation state and especially with the distortion of the local symmetry around the absorber[27] that leads to an increasing *3d-4p* orbital mixing, and thus to a larger overlap of the *3d* vanadium orbital with the *2p* oxygen orbitals.

These spectroscopic signatures are fully consistent with previous observations made for highly oxidized compositions such as $Na_3V_2(PO_4)_2F_{3-y}O_y$ (where y = 1.6 [13, 24] and y = 2.0 [14]) and also with related compounds such as $VOPO_4 \cdot 2H_2O$.[31-32]

NMR

Figure 7 illustrates the ^{23}Na MAS NMR spectrum of $NVPF_3$ recorded at 132.3 MHz under a 11.75 T field. Both nuclear dipolar and first order quadrupolar interactions are partially suppressed by MAS. However for nuclei with a strong quadrupolar constant like ^{23}Na (I = 3/2) located in a non-symmetrical site the second order quadrupolar interaction is affected but not suppressed by MAS, possibly causing some residual broadening to the central transition. The isotropic shift of the ^{23}Na signal is mainly governed by the Fermi contact interaction in such paramagnetic phases; *i.e.* it depends on the electronic spin density at the ^{23}Na nucleus.

The $NVPF_3$ spectrum exhibits two major signals at 91 and 138 ppm with very different magnitude and a set of spinning side bands for each. Liu *et al.*[22] reported a similar spectrum and assigned these peaks to the partially filled Na(2) site and to the fully occupied Na(1) site respectively based on the tetragonal structure described in the space group $P4_2/mnm$ and reported by Le Meins *et al.*[23] As discussed in the following a different assignment for these signals is proposed.

Figure 7 shows the ^{23}Na MAS NMR spectra of the complete series of $NVPF_{3-y}O_y$ compounds from y = 0 ($NVPF_3$) to y = 0.5 ($NVPF_{2.5}O_{0.5}$). In addition to the 138 and 91 ppm signals, a third signal grows around 50 ppm when the amount of oxygen increases. In the meantime, the 138 ppm signal decreases in intensity and broadens (and slightly shifts toward higher values corresponding to more paramagnetic shifts) and the peak at 91 ppm increases and also shifts towards more paramagnetic shifts. The increase of oxygen content in the lattice induces the formation of V^{4+} ions. Since the V^{4+} (t_{2g}^1) ion generally causes a weaker Fermi contact shift than V^{3+} (t_{2g}^2) as it is less paramagnetic, the signals observed at 138, 91 and 50 ppm are respectively assigned to Na interacting with two V^{3+}, with one V^{3+} and one V^{4+}, and with two V^{4+} (all Na sites being surrounded by two V ions). In our study these pairs are respectively depicted as peak 1, peak 2 and peak 3 in **Figure 7**. Note that the effect of one V^{4+} in the environment of Na instead of one V^{3+} is a decrease of the shift by around 45 ppm each time. This assignment is in agreement with the one reported by Serras *et al.*[24] for the mixed F/O composition $Na_3V_2(PO_4)_2F_{1.4}O_{1.6}$ (y = 1.6).

Therefore, our series of spectra strongly suggests that the signal observed at 91 ppm in $NVPF_3$ actually denotes already the presence of small amount of unexpected oxygen defects in the pristine compound induced either by an incomplete reduction of $V^{III}PO_4$ during the synthesis of the precursor or a partial oxidation of the vanadium (or a lack of fluorine) during the annealing of $NVPF_3$. Thus, the isotropic signals recorded for the sodium sites would lead to the single broad signal observed around 138 ppm. Indeed, all sodium sites have a very similar environment in terms of V^{3+} cations (V-Na interatomic distances are in the range [3.17 - 3.69 Å]), suggesting that they all exhibit very close Fermi contact shifts (see **Figure S8** in supplementary information). This is actually confirmed by DFT calculations of the Fermi contact shift of each sodium in the structure using the VASP code with both GGA and GGA+U methods (see **Table S4** in supplementary information). The actual quantity of oxygen defect present in the pristine $NVPF_3$ material cannot be determined accurately from ^{23}Na MAS NMR since one should take into account the intensities in all spinning sidebands that are widely spread around the isotropic signals.

Figure 8 shows the ^{31}P MAS NMR spectra of $NVPF_{3-y}O_y$ at 40.6 MHz under a 2.35 T field. Similarly to what has been observed in ^{23}Na MAS NMR, two signals (at 5983 and 4500 ppm) are observed in the spectrum of $NVPF_3$. These two signals were also reported by Liu *et al.*[22] who assigned the resonance at 5932 ppm to one phosphorous site (again in the assumed $P4_2/mnm$ space group), and the resonance centered at 4500 ppm to the other phosphorous site. In fact, in the actual structure (described in the *Amam* space group), there is only one phosphorous site which shares corners with four VO_4F_2 polyhedra (see **Figure 1** and **Figure S9** in supplementary information). Again, based on the analysis of the $NVPF_{3-y}O_y$ ($0 \leq y \leq 0.5$) series another assignment of the ^{31}P MAS NMR signals is proposed: the five peaks observed at 6097, 4583, 3058, 1565, and ~ 0 ppm are assigned respectively to phosphorous environments with only adjacent V^{3+} ions (peak 1), one V^{4+} and three V^{3+} ions (peak 2), two V^{4+} and two V^{3+} ions (peak 3), three V^{4+} and one V^{3+} ions (peak 4), and only adjacent V^{4+} ions (peak 5). Indeed, the effect of one V^{4+} in the environment of phosphorous instead of one V^{3+} leads to a decrease of the shift by around 1500 ppm each time. In very good agreement with the additional ^{23}Na NMR signal discussed above, our series of spectra then strongly suggests that $NVPF_3$ already exhibits some unexpected oxygen defects in the pristine material.

Figure 8 represents the experimental relative amount of the 5 possible ^{31}P environments (see **Figures S4** to **S7** in supplementary information for the corresponding fit of spectra into individual components using the DMFit code), compared with those expected based on a statistical distribution of V^{4+} ions in $NVPF_{3-y}O_y$ ($0 \leq y \leq 0.5$). The theoretical probabilities were calculated using the binominal distribution (*cf.* Equation 1) which gives the probability for having k occurrences among n possibilities (k = 0, 1, 2, 3, or 4), the probability of each occurrence being p. Here, each phosphorus is surrounded by 4 V (n = 4). Each V has a probability p of being V^{4+}. For each compound the probability p is calculated by $p = y/z$,

where y is the oxygen content in $NVPF_{3-y}O_y$ (y = 0.1, 0.2, 0.3, 0.4, and 0.5) and z = 2 (the total number of vanadium in the unit cell).

Equation 1

$$C\ (n,k)\ p^k\ (1-p)^{(n-k)} = \left(\frac{n!}{k!(n-k)!}\right) p^k (1-p)^{(n-k)}$$

As shown in **Figure 8**, the experimental intensities distribution does not follow the theoretical one if the repartition of V^{3+} and V^{4+} ions would have been statistical around each phosphorous: phosphorous nuclei appear to be experimentally surrounded by more V^{4+} than expected. A possible explanation could be that locally a rapid electronic hopping occurs between V^{n+} ions. So in average the P nuclei would see more V^{4+} ions that theoretically expected.

4. Electrochemical properties

Figure 9 shows the voltage-composition and the associated derivative curves obtained for $Na_{3-x}V_2(PO_4)_2F_{3-y}O_y$ ($0 \leq y \leq 0.5$) during their second cycle in Na batteries at the rate of C/20. These electrochemical data are similar to each other with two main voltage domains around 3.65 and 4.15 V *vs* Na^+/Na and a voltage jump around x = 2 which suggests the presence of a stable intermediate phase for this composition regardless the y value.

Previous studies[11-12, 14, 24] of $Na_{3-x}V_2(PO_4)_2F_{3-y}O_y$ ($0 \leq y \leq 2$) focused on more oxidized compositions (y > 1.5) have demonstrated that the reversible capacity is around 125 mAh/g whatever the fluorine content: as supported by first-principles calculations the extraction of only two Na^+ ions is possible within the voltage range 2 - 4.5 V *vs* Na^+/Na, imposed by the limited stability of electrolytes such as $NaPF_6$ (1M) in EC:DMC (1:1) (3wt% FEC).[14] Parasitic reactions induced by the degradation of the electrolyte during the first cycles (see **Figure S10** for more detailed information), and especially the modification of the Na metal counter electrode's operating voltage due to the formation of unstable passivation layers at its surface[34-35] lead to a lack of accuracy in the quantitative evaluation of the reversible capacity delivered by $Na//NVPF_{3-y}O_y$ half cells. On the contrary, studies performed in full Na-ion cells for $NVPF_3$ *vs* hard carbon have already demonstrated truly excellent reversibility and cyclability.[35-36] It is now well established that, on the contrary to what is true for the lithium technology, electrochemical tests are required in full Na-ion cells to obtain confident evaluation of the electrochemical performance associated to a given active material.[34-35] To address these performances studies in full cells versus hard carbon are currently in progress for $NVPF_{3-y}O_y$ with y > 0 and will be discussed in a forthcoming paper. Here, the discussion of the electrochemical signatures will be limited to their relationship with the materials' compositions and structures in order to reconcile all the apparent discrepancies reported in literature.

As *y* increases (*i.e.* as the fluorine content decreases) the average potential of the cell continuously decreases, as highlighted by the shift of the derivative peaks to lower voltages on **Figure 9**. The average voltage of the cell varies from 3.89 V for $y = 0$ to 3.83 V for $y = 0.5$. It is ascribed to the formation of highly covalent vanadyl-type bonds $(V=O)^{2+}$ at the apex of the bi-octahedra $V_2O_8F_{3-y}O_y$ that "continuously" replace the more ionic V-F bonds as *y* increases. In fact, a more covalent environment for the transition metal ion raises the energy of its antibonding levels closer to the Fermi energy of sodium and thus induces a decrease in voltage for the involved redox couple *vs* Na^+/Na. Even if the redox couples involved in the electrochemical processes are different since oxygen substitution for fluorine induces a partial oxidation of vanadium from the trivalent state to the tetravalent state, the voltage of the whole series of compounds remains quite similar. Indeed, as already observed for the Tavorite phases $LiV^{III}PO_4F$ and $LiV^{IV}PO_4O$[37] the impact of the vanadyl-type bond is major and makes that the redox couple V^{3+}/V^{4+} apparently operates at higher voltage (+ 0.3 V) in $LiVPO_4F$ than the "redox couple" V^{4+}/V^{5+} in $LiVPO_4O$. In fact, V^{4+}/V^{5+} is actually $(V=O)^{2+}/(V=O)^{3+}$ in the case of this oxyphosphate.

The electrochemical voltage-composition data differ significantly in their shape depending on the composition in oxygen: the more oxidized the compound, the "smoother" their cycling profiles. In the low voltage domain (between 3.5 and 3.8 V *vs* Na^+/Na), for $y = 0$ and 0.1 two sharp peaks are clearly observed around 3.7 V in the derivative data whereas for the more oxidized compounds only one broader and asymmetric peak is observed. In the high voltage domain (between 3.9 and 4.3 V), a similar behavior is observed with an evolution from sharp peaks around 4.2 V for $y = 0$ to broader peaks for more oxidized compositions. This emphasizes that a small change in their initial compositions and thus in their vanadium average oxidation states has a major impact on the phase diagram stabilized upon cycling. It evolves from a complex series of biphasic domains and solid solutions for $y = 0$, as determined for $NVPF_3$ by Bianchini *et al.*[15] to an extended solid solution for $y > 0.2$. Complementary *in situ* and *operando* experiments are in progress in order to get more in-depth insights in the phase diagrams stabilized upon cycling as function of *y* (*i.e.* the oxygen substitution ratio for fluorine).

Another noteworthy feature of the electrochemical performances is the decrease of the hysteresis between charge and discharge as *y* increases. This could be qualitatively attributed to better transport properties (ionic and electronic) favored by mixed valence V^{III}/V^{IV} in the pristine material that might favor electronic transfer.

To conclude, this study of a series of partially oxidized compositions $Na_{3-x}V_2(PO_4)_2F_{3-y}O_y$ ($0 \leq y \leq 0.5$) allows to get a better insight in the incoherency reported throughout the literature. For example, Liu *et al.*[22] reported, for a composition announced to be $NVPF_3$ a solid solution mechanism all along the electrochemical process. However, the cell parameters $a = b = 9.04$ Å and $c = 10.735$ Å given suggest a $y = 0.15$ composition, in good agreement with a solid solution reaction upon electrochemical cycling,

according to the results we obtained. Another example is that of Song *et al.*[19] who reported $NVPF_3$ with cell parameters of $a = b = 9.05$ Å and $c = 10.679$ Å. According to our results this material is strongly oxidized and such as $y > 0.5$; this explains why the average voltages are as low as 4 and 3.5 V *vs* Na^+/Na for the two composition domains.

Conclusion

A series of $Na_3V_2(PO_4)_2F_{3-y}O_y$ compositions with $0 \leq y \leq 0.5$ has been successfully synthesized by controlling the oxidation state of the VPO_4 and $VOPO_4$ precursors, as well as the F/O ratio using the stoichiometric mixture $(3-y)NaF/(y/2)Na_2CO_3$. An in-depth structural characterization has revealed that all of them are isostructural and crystallize in the orthorhombic space group *Amam* with an increasing disorder in the Na^+ ions distribution. Indeed, an additional crystallographic site with a significant occupancy (up to 16 % for $y = 0.5$) is required to fully describe the localization of the Na^+ ions within the channels of this three-dimensional framework of the oxidized compound. When $Na_3V_2(PO_4)_2F_{3-y}O_y$ is partially oxidized the sodium distribution become "mid-way" between those obtained at room temperature and at high temperature for $Na_3V_2(PO_4)_2F_3$ ($y = 0$) by Bianchini *et al.*[16] Combination of XANES and NMR spectroscopies has confirmed the charge compensation of oxygen substitution for fluorine is achieved by the continuous oxidation of vanadium and the continuous formation of vanadyl-type bonds, but it has also revealed a tendency to adopt a non-statistical V^{4+} distribution within the framework, as well as the presence of a few V^{4+}-type defects already in the compound considered to be "non-oxidized". As already shown for other materials of interest for batteries such as $LiCoO_2$[38] and $LiVPO_4F$[39] NMR spectroscopy as a local probe of the bulk appears often as the technique of choice to identify the presence of defects. Indeed, single ^{23}Na and ^{31}P MAS NMR signals are in fact associated to the different crystallographic sites observed for Na and P in the structure of $Na_3V_2(PO_4)_2F_3$ ($y = 0$), the additional signals at 91 ppm (for ^{23}Na) and at 5983 ppm (for ^{31}P) being due to V^{4+} defects in their close environments. Finally, this study has allowed, considering a partial oxygen substitution for fluorine, to understand all the apparent discrepancies reported in the literature for $Na_3V_2(PO_4)_2F_3$ ($y = 0$). With an increase of oxygen content, the electrochemical signature of $Na_3V_2(PO_4)_2F_{3-y}O_y$ with $0 \leq y \leq 0.5$ evolves from a complex phase diagram with two voltage plateaus for $y = 0$ to solid solution type reactions with a "S-shape" for the two voltage domains for $y = 0.5$. In fact, most of the materials reported as $Na_3V_2(PO_4)_2F_3$ in the literature are in fact partially oxidized, with a decrease of the average voltage and thus of the theoretical energy density.

Supporting Information

Additional information on the powder morphology, structure (SXRD and NMR) and electrochemical characterization. This material is available free of charge via the Internet at http://pubs.acs.org/.

Acknowledgments

The authors thank Philippe Dagault, Cathy Denage and Laetitia Etienne at ICMCB for technical assistance, Rénald David at LRCS for the preparation of the electrolyte, as well as ALBA (Barcelona, Spain) for Synchrotron X-ray diffraction and absorption experiments on MSPD and CLÆSS beamlines. The authors also acknowledge RS2E for the funding of TB's postdoctoral fellowship. This project has received funding from Région Aquitaine, the French National Research Agency (STORE-EX Labex Project ANR-10-LABX-76-01 and SODIUM Descartes project ANR-13-RESC-0001-02), and the European Union's Horizon 2020 research and innovation programme under grant agreement No 646433-NAIADES. The Mésocentre de Calcul Intensif Aquitain (MCIA) and the modelling center of ISM are acknowledged for computing facilities.

References

1. Armand, M.; Tarascon, J.-M., Building better batteries. *Nature* **2008,** *451*, 652-657.
2. Tarascon, J.-M., Is lithium the new gold? *Nature Chem.* **2010,** *2*, 510.
3. Palomares, V.; Serras, P.; Villaluenga, I.; Hueso, K. B.; Carretero-González, J.; Rojo, T., Na-ion batteries, recent advances and present challenges to become low cost energy storage systems. *Energy Environ. Sci.* **2012,** *5*, 5884-5901.
4. Jian, Z.; Han, W.; Lu, X.; Yang, H.; Hu, Y. S.; Zhou, J.; Zhou, Z.; Li, J.; Chen, W.; Chen, D., Superior Electrochemical Performance and Storage Mechanism of $Na_3V_2(PO_4)_3$ Cathode for Room-Temperature Sodium-Ion Batteries. *Adv. Eng. Mater.* **2013,** *3*, 156-160.
5. Sauvage, F.; Quarez, E.; Tarascon, J.-M.; Baudrin, E., Crystal structure and electrochemical properties vs. Na^+ of the sodium fluorophosphate $Na_{1.5}VOPO_4F_{0.5}$. *Solid State Sci.* **2006,** *8*, 1215-1221.
6. Shakoor, R.; Seo, D.-H.; Kim, H.; Park, Y.-U.; Kim, J.; Kim, S.-W.; Gwon, H.; Lee, S.; Kang, K., A combined first principles and experimental study on $Na_3V_2(PO_4)_2F_3$ for rechargeable Na batteries. *J. Mat. Chem.* **2012,** *22*, 20535-20541.
7. LIU, Z.-m.; WANG, X.-y.; Ying, W.; TANG, A.-p.; YANG, S.-y.; HE, L.-f., Preparation of $NaV_{1-x}Al_xPO_4F$ cathode materials for application of sodium-ion battery. *T. Nonferr. Metal. Soc.* **2008,** *18*, 346-350.
8. Chihara, K.; Kitajou, A.; Gocheva, I. D.; Okada, S.; Yamaki, J.-i., Cathode properties of $Na_3M_2(PO_4)_2F_3$ [M= Ti, Fe, V] for sodium-ion batteries. *J. Power Sources* **2013,** *227*, 80-85.
9. Kim, H.; Shakoor, R.; Park, C.; Lim, S. Y.; Kim, J. S.; Jo, Y. N.; Cho, W.; Miyasaka, K.; Kahraman, R.; Jung, Y., Na2FeP2O7 as a Promising Iron-Based Pyrophosphate Cathode for Sodium Rechargeable Batteries: A Combined Experimental and Theoretical Study. *Adv. Funct. Mater.* **2013,** *23*, 1147-1155.
10. Masquelier, C.; Croguennec, L., Polyanionic (phosphates, silicates, sulfates) frameworks as electrode materials for rechargeable Li (or Na) batteries. *Chem. Rev.* **2013,** *113*, 6552-6591.
11. Serras, P.; Palomares, V.; Goñi, A.; de Muro, I. G.; Kubiak, P.; Lezama, L.; Rojo, T., High voltage cathode materials for Na-ion batteries of general formula $Na_3V_2O_{2x}(PO_4)_2F_{3-2x}$. *J. Mat. Chem.* **2012,** *22*, 22301-22308.
12. Serras, P.; Palomares, V.; Goñi, A.; Kubiak, P.; Rojo, T., Electrochemical performance of mixed valence $Na_3V_2O_{2x}(PO_4)_2F_{3-2x}$/C as cathode for sodium-ion batteries. *J. Power Sources* **2013,** *241*, 56-60.

13. Park, Y.-U.; Seo, D.-H.; Kwon, H.-S.; Kim, B.; Kim, J.; Kim, H.; Kim, I.; Yoo, H.-I.; Kang, K., A new high-energy cathode for a Na-ion battery with ultrahigh stability. *J. Am. Chem. Soc.* **2013,** *135*, 13870-13878.
14. Park, Y. U.; Seo, D. H.; Kim, H.; Kim, J.; Lee, S.; Kim, B.; Kang, K., A Family of High-Performance Cathode Materials for Na-ion Batteries, $Na_3(VO_{1-x}PO_4)_2F_{1+2x}$ $(0 \leq x \leq 1)$: Combined First-Principles and Experimental Study. *Adv. Funct. Mater.* **2014,** *24*, 4603-4614.
15. Bianchini, M.; Fauth, F.; Brisset, N.; Weill, F.; Suard, E.; Masquelier, C.; Croguennec, L., Comprehensive Investigation of the $Na_3V_2(PO_4)_2F_3$ – $NaV_2(PO_4)_2F_3$ System by Operando High Resolution Synchrotron X-ray Diffraction. *Chem. Mater.* **2015,** *27*, 3009-3020.
16. Bianchini, M.; Brisset, N.; Fauth, F.; Weill, F.; Elkaim, E.; Suard, E.; Masquelier, C.; Croguennec, L., $Na_3V_2(PO_4)_2F_3$ revisited: a high-resolution diffraction study. *Chem. Mater.* **2014,** *26*, 4238-4247.
17. Tsirlin, A.; Nath, R.; Abakumov, A.; Furukawa, Y.; Johnston, D.; Hemmida, M.; von Nidda, H.-A. K.; Loidl, A.; Geibel, C.; Rosner, H., Phase separation and frustrated square lattice magnetism of $Na_{1.5}VOPO_4F_{0.5}$. *Phys. Rev. B* **2011,** *84*, 014429.
18. Gover, R.; Bryan, A.; Burns, P.; Barker, J., The electrochemical insertion properties of sodium vanadium fluorophosphate, $Na_3V_2(PO_4)_2F_3$. *Solid State Ionics* **2006,** *177*, 1495-1500.
19. Song, W.; Ji, X.; Wu, Z.; Zhu, Y.; Li, F.; Yao, Y.; Banks, C. E., Multifunctional dual $Na_3V_2(PO_4)_2F_3$ cathode for both lithium-ion and sodium-ion batteries. *RSC Advances* **2014,** *4*, 11375-11383.
20. Barker, J.; Gover, R.; Burns, P.; Bryan, A., Hybrid-ion a lithium-ion cell based on a sodium insertion material. *Electrochem. Solid St.* **2006,** *9*, A190-A192.
21. Barker, J.; Gover, R.; Burns, P.; Bryan, A., $Li_{4/3}Ti_{5/3}O_4$ ‖ $Na_3V_2(PO_4)_2F_3$: An Example of a Hybrid-Ion Cell Using a Non-graphitic Anode. *J. Electrochem. Soc.* **2007,** *154*, A882-A887.
22. Liu, Z.; Hu, Y.-Y.; Dunstan, M. T.; Huo, H.; Hao, X.; Zou, H.; Zhong, G.; Yang, Y.; Grey, C. P., Local Structure and Dynamics in the Na Ion Battery Positive Electrode Material $Na_3V_2(PO_4)_2F_3$. *Chem. Mater.* **2014,** *26*, 2513-2521.
23. Le Meins, J.-M.; Crosnier-Lopez, M.-P.; Hemon-Ribaud, A.; Courbion, G., Phase transitions in the $Na_3M_2(PO_4)_2F_3$family (M= Al 3+, V 3+, Cr 3+, Fe 3+, Ga 3+): synthesis, thermal, structural, and magnetic studies. *J. Solid State Chem.* **1999,** *148*, 260-277.
24. Serras, P.; Palomares, V.; Alonso, J.; Sharma, N.; López del Amo, J. M.; Kubiak, P.; Fdez-Gubieda, M. L.; Rojo, T. f., Electrochemical Na Extraction/Insertion of $Na_3V_2O_{2x}(PO_4)_2F_{3-2x}$. *Chem. Mater.* **2013,** *25*, 4917-4925.
25. Koningsberger, D.; Prins, R., X-ray absorption: principles, applications, techniques of EXAFS, SEXAFS, and XANES. **1988**.
26. Park, Y.-U.; Seo, D.-H.; Kim, B.; Hong, K.-P.; Kim, H.; Lee, S.; Shakoor, R. A.; Miyasaka, K.; Tarascon, J.-M.; Kang, K., Tailoring a fluorophosphate as a novel 4 V cathode for lithium-ion batteries. *Scientific reports* **2012,** *2*.
27. Wong, J.; Lytle, F.; Messmer, R.; Maylotte, D., K-edge absorption spectra of selected vanadium compounds. *Phys. Rev. B* **1984,** *30*, 5596.
28. Stizza, S.; Mancini, G.; Benfatto, M.; Natoli, C.; Garcia, J.; Bianconi, A., Structure of oriented V_2O_5 gel studied by polarized x-ray-absorption spectroscopy at the vanadium K edge. *Phys. Rev. B* **1989,** *40*, 12229.
29. Šipr, O.; Šimůnek, A.; Bocharov, S.; Kirchner, T.; Dräger, G., Geometric and electronic structure effects in polarized V K-edge absorption near-edge structure spectra of V_2O_5. *Phys. Rev. B* **1999,** *60*, 14115.
30. Mansour, A.; Smith, P.; Baker, W.; Balasubramanian, M.; McBreen, J., In situ XAS investigation of the oxidation state and local structure of vanadium in discharged and charged V_2O_5 aerogel cathodes. *Electrochim. Acta* **2002,** *47*, 3151-3161.
31. Poumellec, B.; Kraizman, V.; Aifa, Y.; Cortes, R.; Novakovich, A.; Vedrinskii, R., Experimental and theoretical studies of dipole and quadrupole contributions to the vanadium K-edge XANES for $VOPO_4{\cdot}2H_2O$ xerogel. *Phys. Rev. B* **1998,** *58*, 6133.
32. Chauvel, B.; Bondot, P.; de Roy, M.; Besse, J. In Spectroscopic Study of $VOPO_4{\cdot}2H_2O$ Intercalation Compounds, *Mater. Sci. Forum, Trans. Tech. Publ.* **1992**, 351-356.

33. Salem, S.; Chang, C.-N.; Nash, T., Energy shift and structure of the K-absorption edge of vanadium in some vanadium compounds. *Physical Review B* **1978,** *18*, 5168.
34. Rudola, A.; Aurbach, D.; Balaya, P., A new phenomenon in sodium batteries: Voltage step due to solvent interaction. *Electrochem. Comm.* **2014,** *46*, 56-59.
35. Dugas, R.; Zhang, B.; Rozier, P.; Tarascon, J., Optimization of Na-Ion Battery Systems Based on Polyanionic or Layered Positive Electrodes and Carbon Anodes. *J. The Electrochem. Soc.* **2016,** *163*, A867-A874.
36. Ponrouch, A.; Dedryvère, R.; Monti, D.; Demet, A. E.; Mba, J. M. A.; Croguennec, L.; Masquelier, C.; Johansson, P.; Palacín, M. R., Towards high energy density sodium ion batteries through electrolyte optimization. *Energy Environ. Sci.* **2013,** *6*, 2361-2369.
37. Ateba Mba, J.-M.; Masquelier, C.; Suard, E.; Croguennec, L., Synthesis and crystallographic study of homeotypic $LiVPO_4F$ and $LiVPO_4O$. *Chem. Mater.* **2012,** *24*, 1223-1234.
38. Levasseur, S.; Ménétrier, M.; Shao-Horn, Y.; Gautier, L.; Audemer, A.; Demazeau, G.; Largeteau, A.; Delmas, C., Oxygen vacancies and intermediate spin trivalent cobalt ions in lithium-overstoichiometric $LiCoO_2$. *Chem. Mater.* **2003,** *15*, 348-354.
39. Messinger, R. J.; Ménétrier, M.; Salager, E.; Boulineau, A.; Duttine, M.; Carlier, D.; Ateba Mba, J.-M.; Croguennec, L.; Masquelier, C.; Massiot, D., Revealing Defects in Crystalline Lithium-Ion Battery Electrodes by Solid-State NMR: Applications to $LiVPO_4F$. *Chem. Mater.* **2015,** *27*, 5212-5221.

Table caption

Table 1: Cell parameters determined from the profile matching of SXRD data considering a unit cell described in the orthorhombic *Amam* space group. The corresponding chemical analyses performed by ICP-OES are also given for information.

Figure captions

Figure 1: Top: Three dimensional framework of $NVPF_{3-y}O_y$ where the dark blue atoms emphasize the substitution site of oxygen for fluorine. In red are highlighted the (a,b) planes where the Na^+ ions are contained - Bottom: two possible Na distributions depending on the space group considered to describe the structure, the fraction of filling in red of the Na atom highlights the partial occupancy of the crystallographic site.

Figure 2: Top: comparison of the experimental synchrotron XRD patterns recorded for the six samples $Na_3V_2(PO_4)_2F_{3-y}O_y$ ($0 \leq y \leq 0.5$) - Bottom angular ranges [9.8 - 10.4°] and [24.15 - 24.55°] are given for easier comparison. The indexation of the diffraction lines is given in the *Amam* space group reported for $Na_3V_2(PO_4)_2F_3$ by Bianchini et al.

Figure 3: Changes in the structural parameters as function of the oxygen substitution for fluorine in $NVPF_{3-y}O_y$ considering the description of the structure in the orthorhombic unit cell (*Amam*).

Figure 4: Profile matching of SXRD data obtained for the y = 0.5 compound using *$P4_2/mnm$* and *Amam* space groups.

Figure 5: Fourier difference maps and associated sodium distribution in the y= 0.5 sample obtained with *$P4_2/mnm$* (top) and *Amam* (bottom) space groups

Figure 6: Vanadium K-edge XANES spectra of the samples $Na_3V_2(PO_4)_2F_{3-y}O_y$ ($0 \leq y \leq 0.5$). The insets show an enlarged graph of the pre-edge region and the associated integrated intensity.

Figure 7: Top: ^{23}Na MAS spectra NMR of $Na_3V_2(PO_4)_2F_3$ recorded with a 30 kHz spinning rate and a 11.75 T magnetic field – Bottom: comparison of ^{23}Na MAS NMR spectra for $Na_3V_2(PO_4)_2F_{3-x}O_x$ ($0 \leq y \leq 0.5$)

Figure 8: Top: ^{31}P MAS spectra NMR of $Na_3V_2(PO_4)_2F_{3-y}O_y$ ($0 \leq y \leq 0.5$) recorded with a 30 kHz spinning rate and under a 2.35 T magnetic field – Bottom: comparison between the experimental distributions of V^{3+}/V^{4+} environments around P sites for $Na_3V_2(PO_4)_2F_{3-y}O_y$ ($0 \leq y \leq 0.5$) and the calculated ones by a binominal distribution.

Figure 9: Top: second voltage-composition curve of $Na_{3-x}V_2(PO_4)_2F_{3-y}O_y$ ($0 \leq y \leq 0.5$) cycled at C/20 between 2.5 and 4.3 V – Bottom: associated derivative curves

Table 1. Cell parameters determined from the profile matching of SXRD data considering a unit cell described in the orthorhombic *Amam* space group. The corresponding chemical analyses performed by ICP-OES are also given for information.

	y = 0	y = 0.1	y = 0.2	y = 0.3	y = 0.4	y = 0.5
Unit cell parameters (Å) - Space group: *Amam*						
a	9.0306(1)	9.0308(1)	9.0322(1)	9.0336(1)	9.0337(1)	9.0353(1)
b	9.0450(1)	9.0429(1)	9.0412(1)	9.0396(1)	9.0383(1)	9.0375(1)
c	10.7538(1)	10.7389(1)	10.7213(1)	10.7065(1)	10.6962(1)	10.6863(1)
V	878.393(1)	876.993(1)	875.540(1)	874.304(1)	873.349(1)	872.604(1)
Chemical analyses - Molar ratio						
Na/V	1.3(2)	1.3(2)	1.5(2)	1.5(2)	1.5(2)	1.5(2)
Na/P	1.4(1)	1.4(1)	1.4(1)	1.5(1)	1.4(1)	1.5(1)
V/P	1.02(5)	1.01(5)	1.00(5)	0.99(5)	0.95(5)	0.99(5)

Figure 1

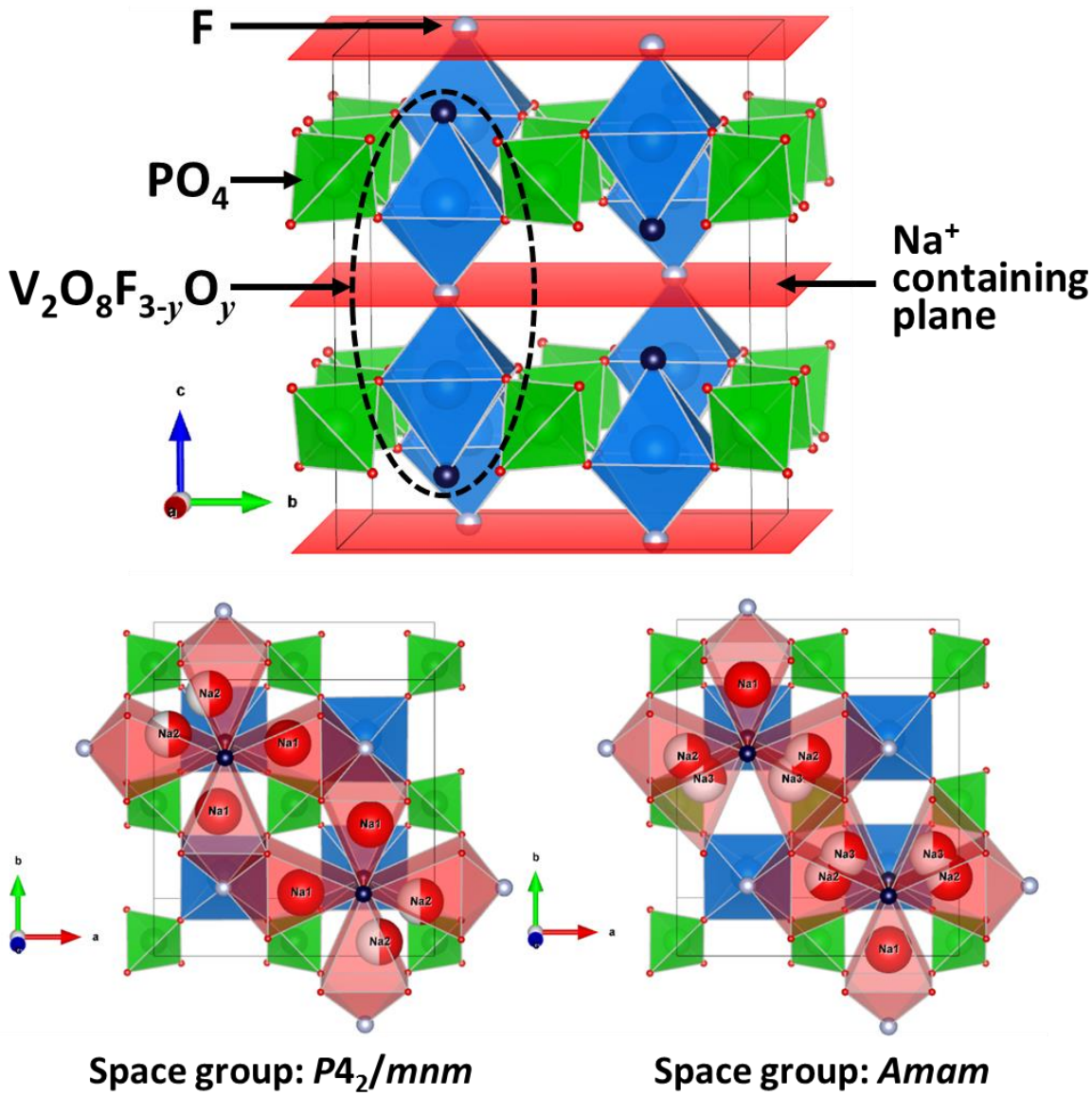
F
PO4
V2O8F3-yOy
Na+ containing plane
c
b
Na2
Na1
Na3
Space group: P42/mnm
Space group: Amam

Figure 2

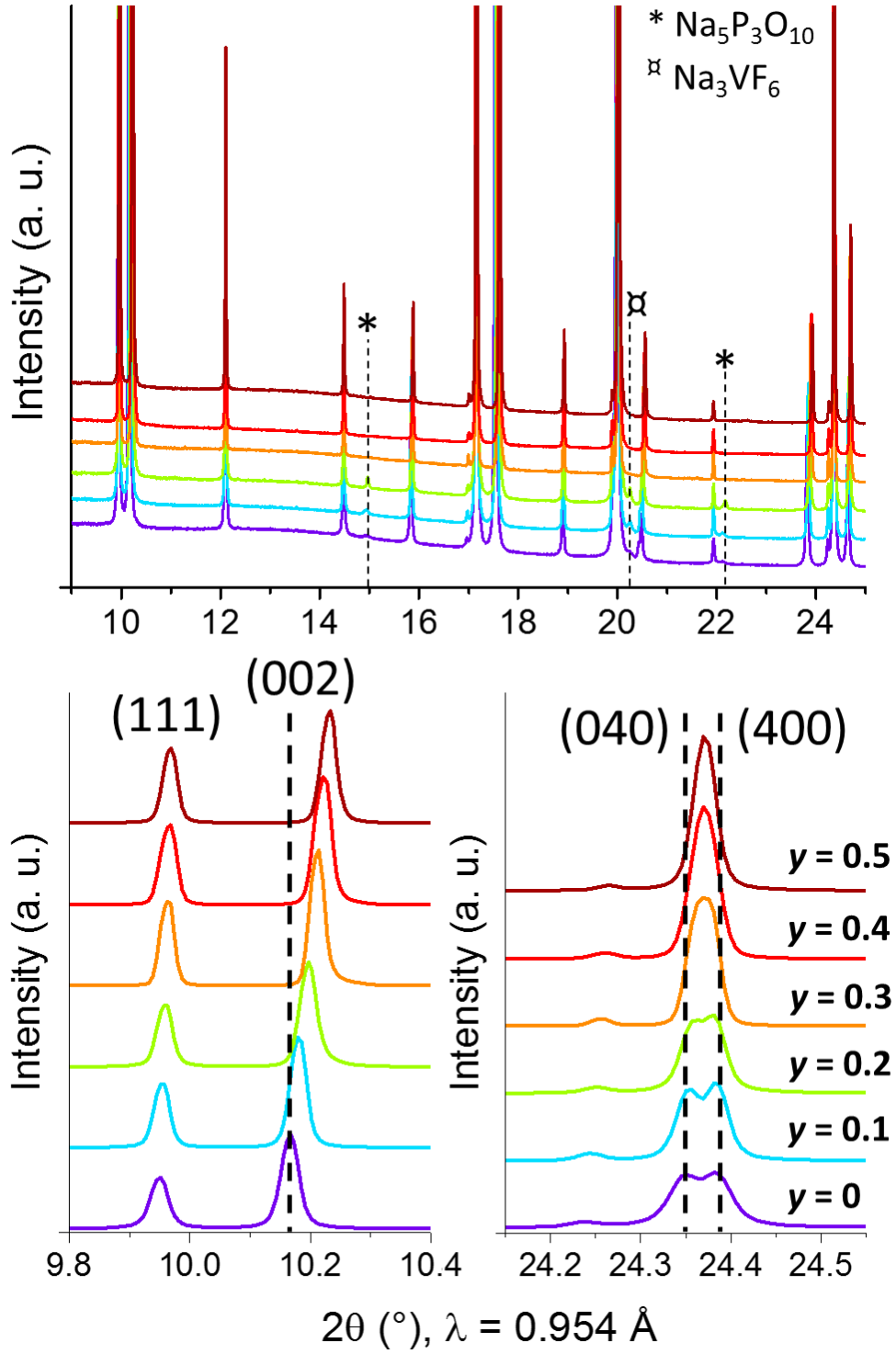
* $Na_5P_3O_{10}$
¤ Na_3VF_6
Intensity (a. u.)
10
12
14
16
18
20
22
24
(111)
(002)
(040)
(400)
y = 0.5
y = 0.4
y = 0.3
y = 0.2
y = 0.1
y = 0
9.8
10.0
10.2
10.4
24.2
24.3
24.4
24.5
2θ (°), λ = 0.954 Å

Figure 3

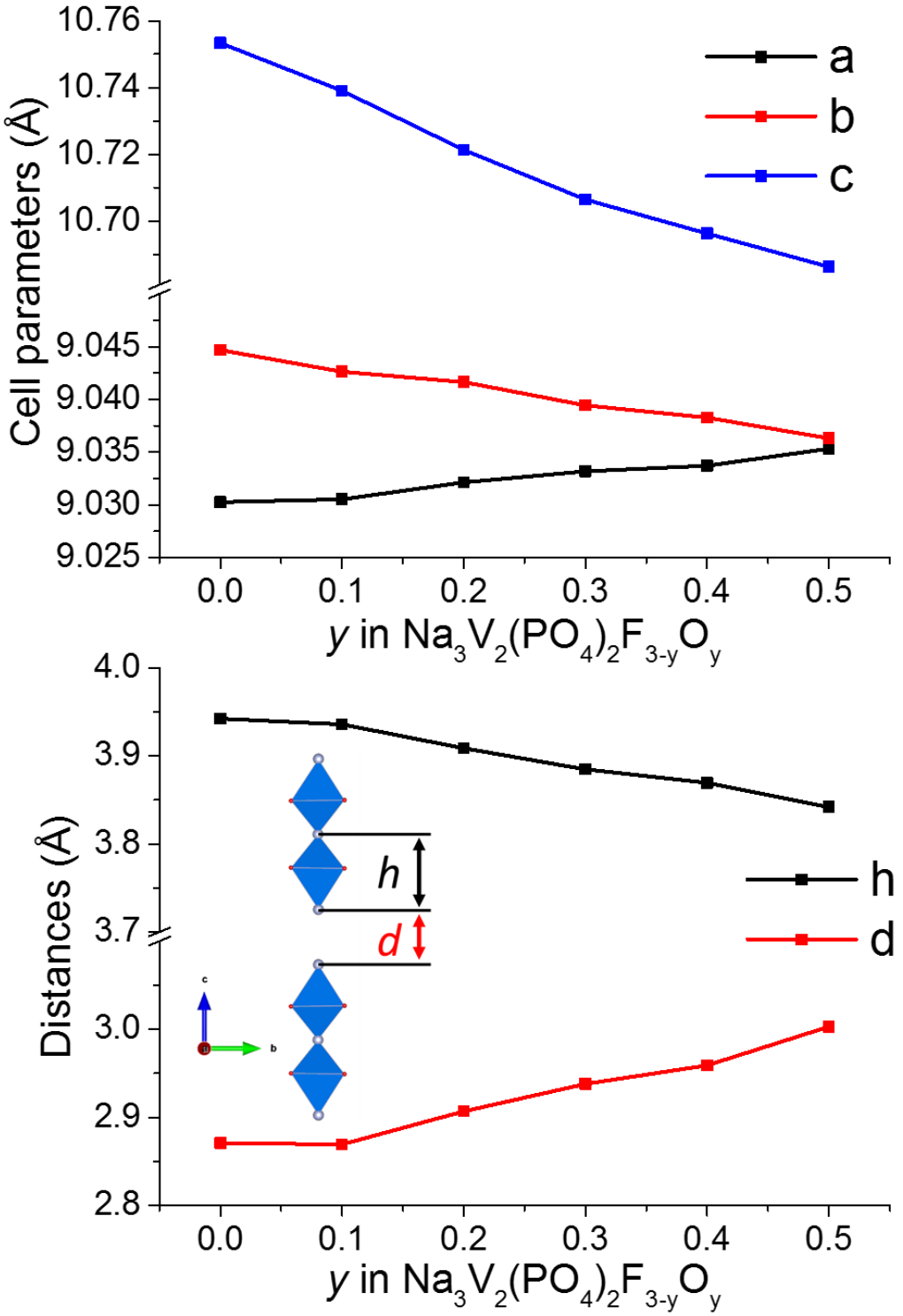
Cell parameters (Å)
10.76
10.74
10.72
10.70
9.045
9.040
9.035
9.030
9.025
a
b
c
0.0
0.1
0.2
0.3
0.4
0.5
y in Na3V2(PO4)2F3-yOy
Distances (Å)
4.0
3.9
3.8
3.7
3.0
2.9
2.8
h
d
h
d
c
b
0.0
0.1
0.2
0.3
0.4
0.5
y in Na3V2(PO4)2F3-yOy

Figure 4

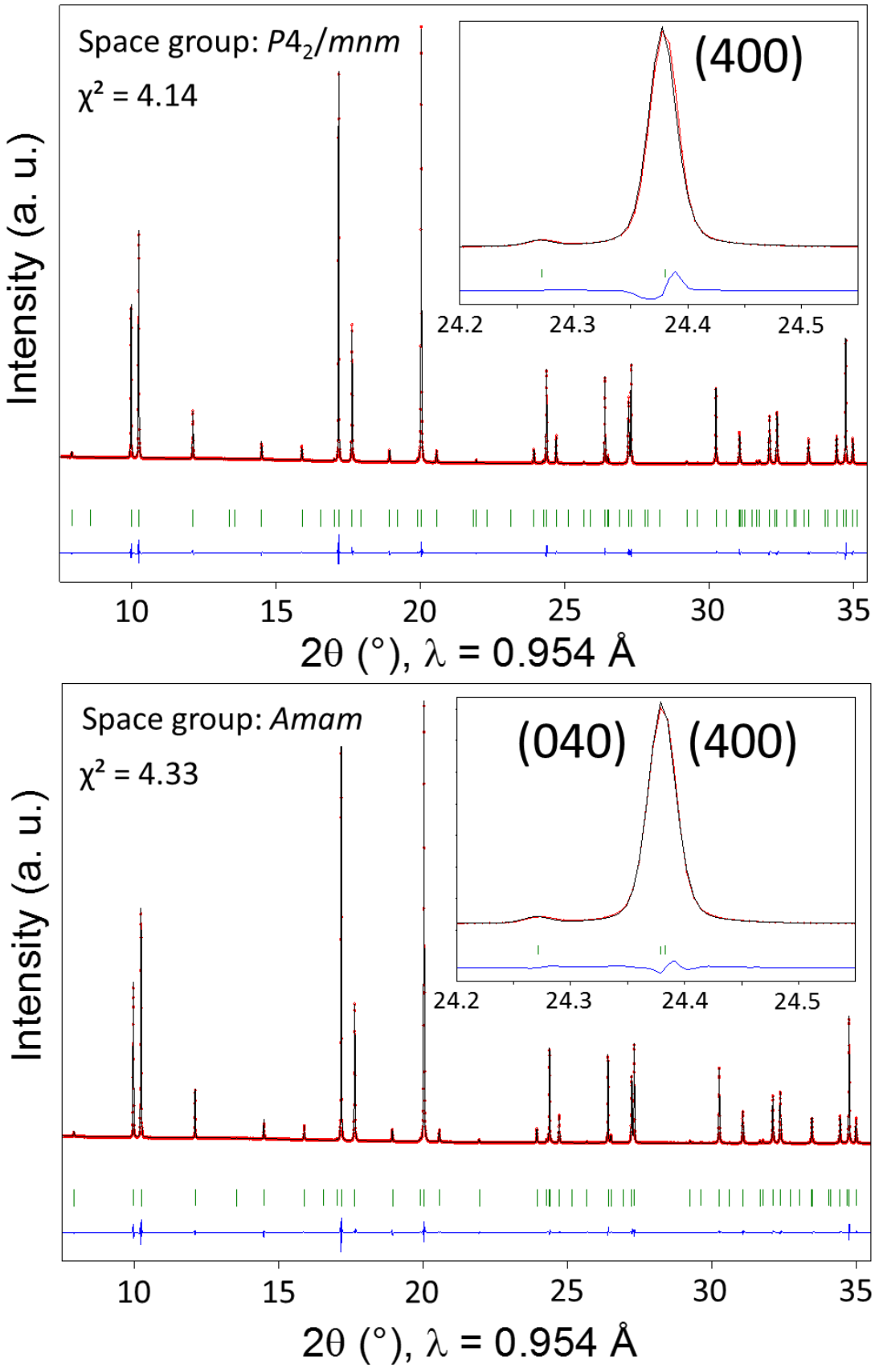
Space group: $P4_2/mnm$
χ^2 = 4.14
(400)
24.2
24.3
24.4
24.5
Intensity (a. u.)
10
15
20
25
30
35
2θ (°), λ = 0.954 Å
Space group: *Amam*
χ^2 = 4.33
(040)
(400)
24.2
24.3
24.4
24.5
Intensity (a. u.)
10
15
20
25
30
35
2θ (°), λ = 0.954 Å

Figure 5

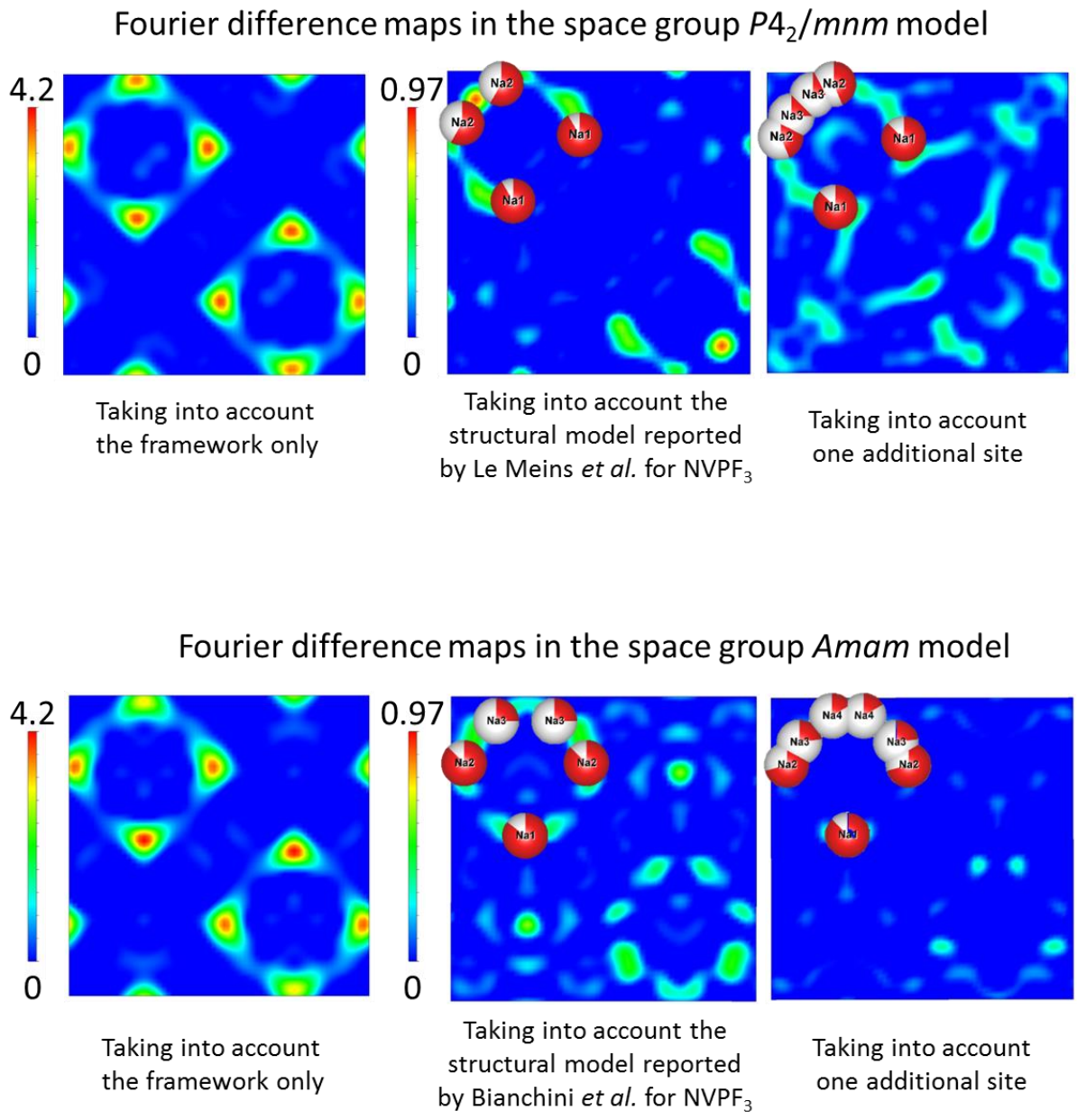
Fourier difference maps in the space group $P4_2/mnm$ model
4.2
0
0.97
0
Na2
Na1
Na3
Taking into account the framework only
Taking into account the structural model reported by Le Meins *et al.* for $NVPF_3$
Taking into account one additional site
Fourier difference maps in the space group *Amam* model
4.2
0
0.97
0
Na3
Na2
Na1
Na4
Taking into account the framework only
Taking into account the structural model reported by Bianchini *et al.* for $NVPF_3$
Taking into account one additional site

Figure 6

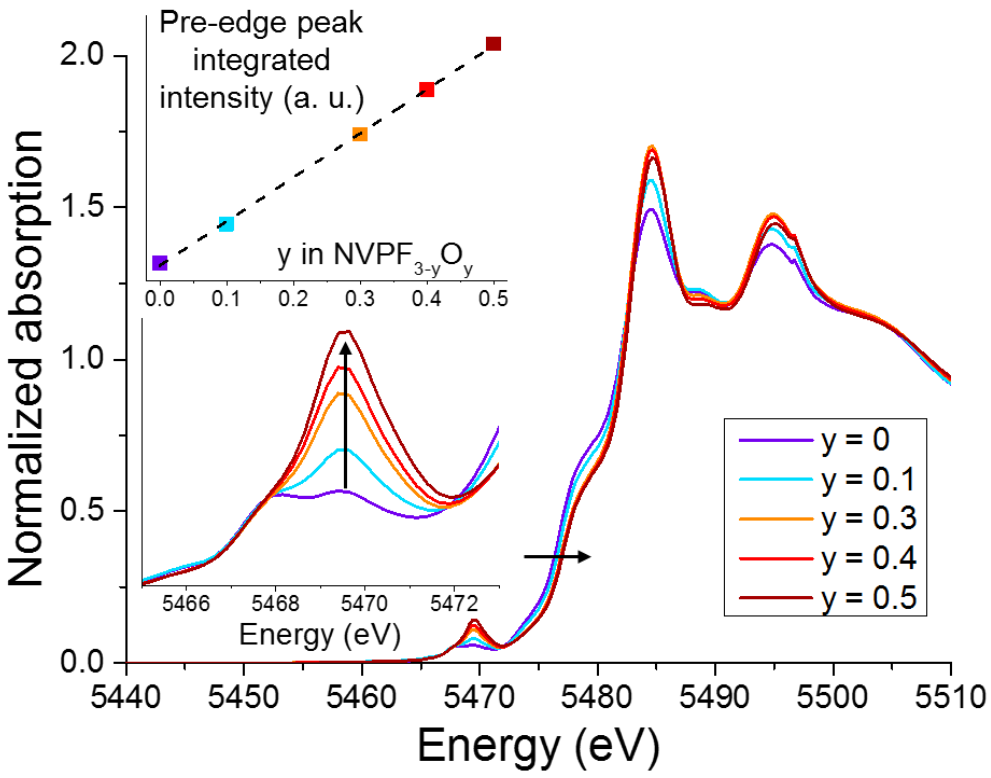
Pre-edge peak
integrated
intensity (a. u.)
y in NVPF3-yOy
0.0
0.1
0.2
0.3
0.4
0.5
5466
5468
5470
5472
Energy (eV)
Normalized absorption
2.0
1.5
1.0
0.5
0.0
5440
5450
5460
5470
5480
5490
5500
5510
Energy (eV)
y = 0
y = 0.1
y = 0.3
y = 0.4
y = 0.5

Figure 7

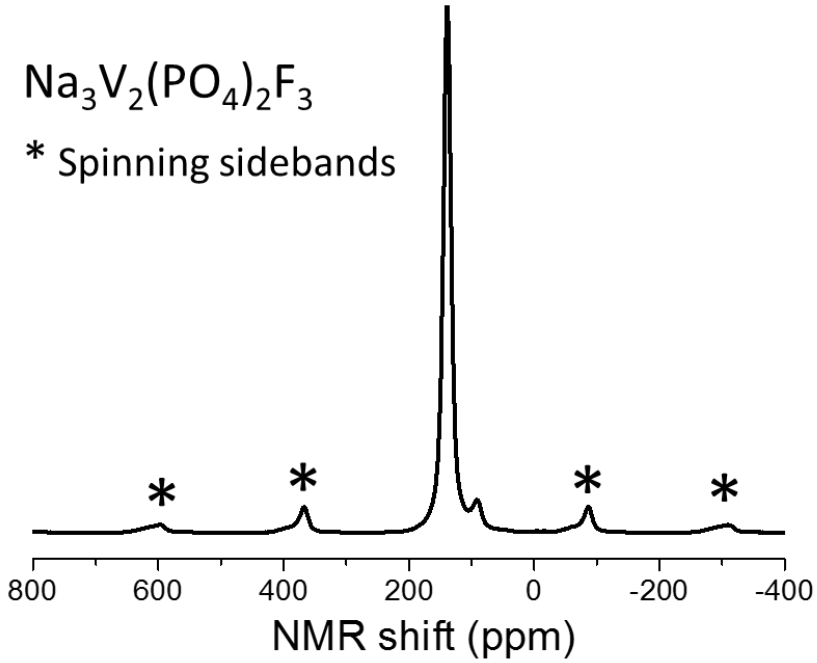
Na3V2(PO4)2F3
* Spinning sidebands
800
600
400
200
0
-200
-400
NMR shift (ppm)

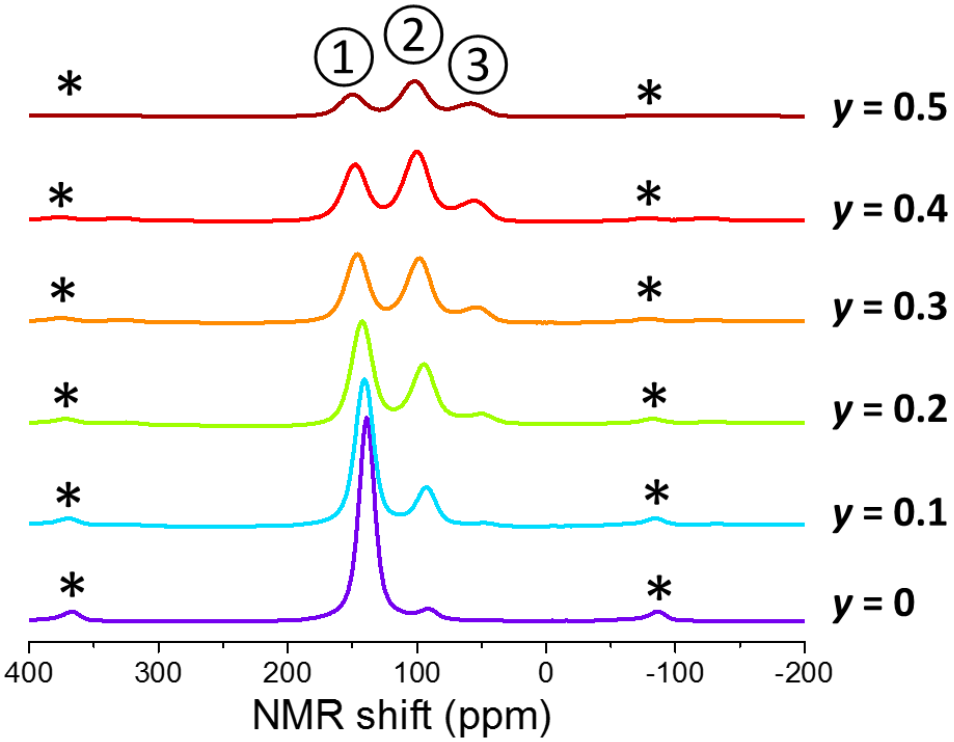
1
2
3
y = 0.5
y = 0.4
y = 0.3
y = 0.2
y = 0.1
y = 0
400
300
200
100
0
-100
-200
NMR shift (ppm)

Figure 8

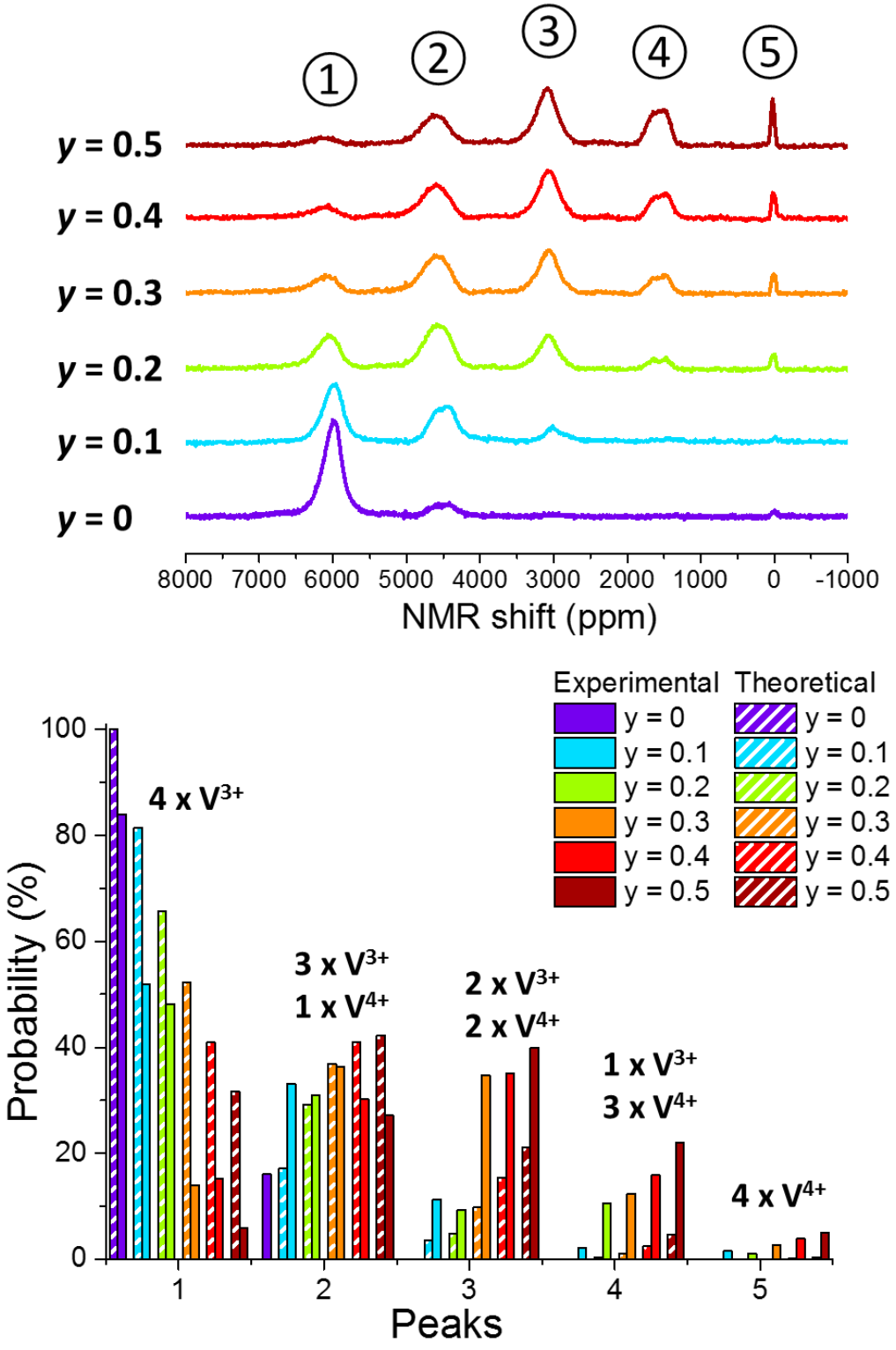
1
2
3
4
5
y = 0.5
y = 0.4
y = 0.3
y = 0.2
y = 0.1
y = 0
8000 7000 6000 5000 4000 3000 2000 1000 0 -1000
NMR shift (ppm)
Experimental
Theoretical
y = 0
y = 0.1
y = 0.2
y = 0.3
y = 0.4
y = 0.5
Probability (%)
100
80
60
40
20
0
4 x V3+
3 x V3+
1 x V4+
2 x V3+
2 x V4+
1 x V3+
3 x V4+
4 x V4+
1
2
3
4
5
Peaks

Figure 9

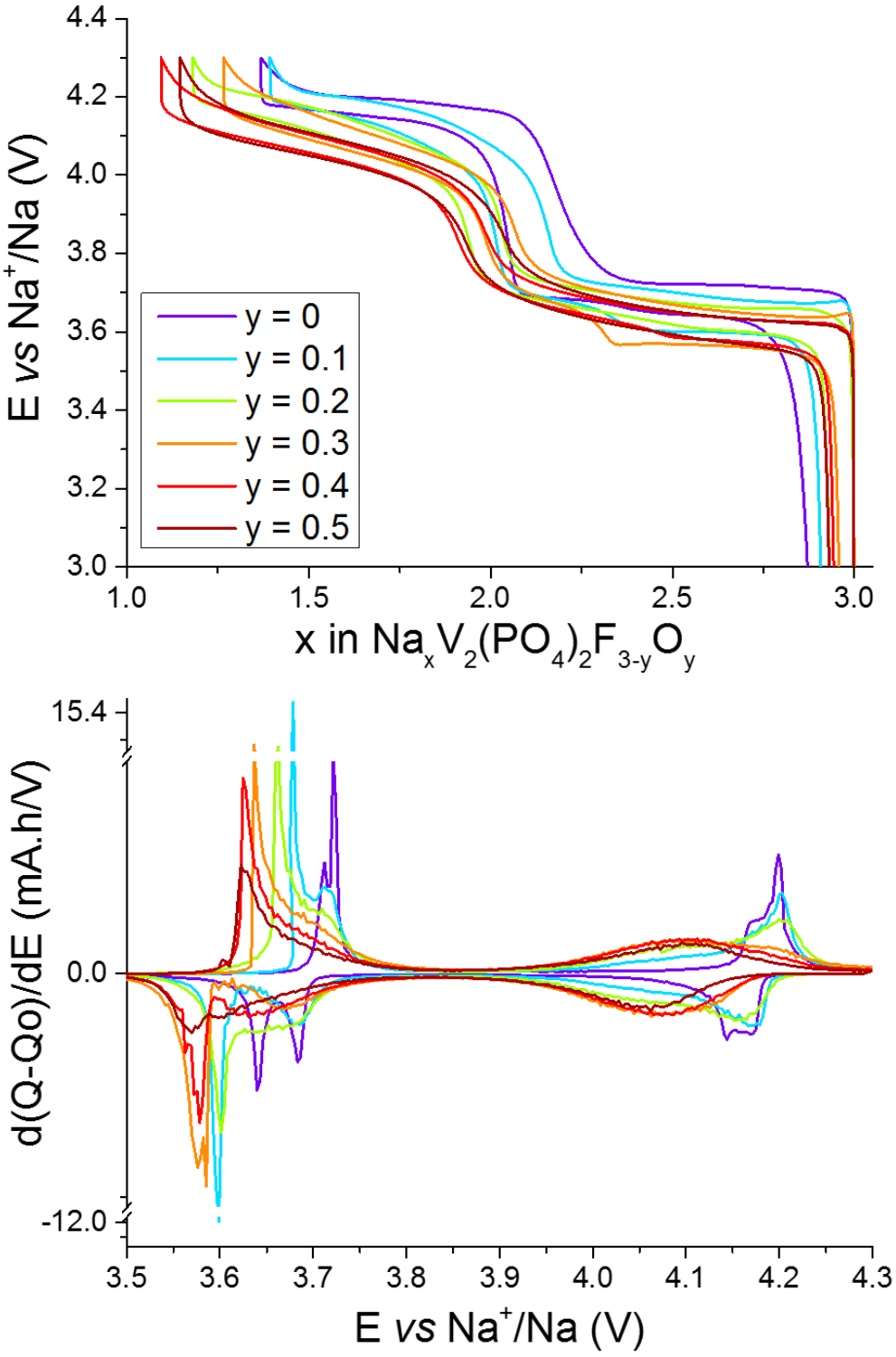
E vs Na+/Na (V)
x in NaxV2(PO4)2F3-yOy
y = 0
y = 0.1
y = 0.2
y = 0.3
y = 0.4
y = 0.5
d(Q-Qo)/dE (mA.h/V)
E vs Na+/Na (V)